Letters

A Smooth-Output Dynamic Wireless Charging System for Automated Guided Vehicles With Dual-Receiver Magnetic Coupler

Yiming Zhang, *Senior Member, IEEE*, Hangyan Zhou, Ronghuan Xie, Xingkui Mao, Xiaoying Chen, and Zhongqi Li

***Abstract*—Dynamic wireless power transmission (DWPT) is a promising technology as it reduces the battery capacity carried by automated guided vehicles and lowers its cost and weight. However, there are large mutual inductance and power fluctuation in the dynamic charging process. In order to solve this problem, this letter proposes a low-cost and low-fluctuation dual-receiver magnetic coupler, which is connected in parallel by two half-bridge rectifiers. The transmitter employs an I-type solenoid coil to enhance the magnetic field and improve the coupling. The optimized design of the coupler structure enables the system to have smooth mutual inductance fluctuation by switching the two receiving coils with each other during the dynamic charging process. The experimental results show that the measured equivalent mutual inductance fluctuation is 3.6%, which verifies the feasibility of the optimized design of the magnetic coupling structure and the effectiveness of the proposed DWPT system.**

***Index Terms*—Automated guided vehicles (AGVs), dual receiver (Rx), dynamic wireless power transfer (DWPT), smooth mutual inductance fluctuation.**

I. Introduction

WIRELESS power transfer (WPT) enables contactless charging and has been widely used in electric vehicles [1], [2], [3] autonomous underwater vehicles [4], implantable biomedical devices [5], and automated guided vehicles (AGVs) [6], due to its advantages of safety, flexibility, and convenience. Among them, the AGV, as a cutting-edge product in modern automation, has the advantages of flexible path and compact structure. It has been widely used in logistics industry and factories, accelerating the development of uncrewed industry.

WPT technology provides a noncontact, isolated, and secure method of power delivery to AGVs, where charging scenarios are mainly categorized into static charging [7], [8], [9] and dynamic charging [10], [11], [12], [13]. Dynamic wireless power transfer (DWPT) enables real-time charging of AGVs during movement [14], which reduces the capacity of batteries carried by AGVs, lowers the cost and weight of AGVs, and greatly improves their utilization efficiency.

Depending on the structure of the transmitter (Tx), DWPT systems are able to be categorized into long-track [15], [16], [17], [18] and short-segmented Tx [19], [20], [21], where the latter has the advantages of high efficiency and lower electromagnetic interference and, thus, has been more widely used. Multiple rectangular unipolar coils are used as Txs to dynamically charge the vehicle [18], but the close arrangement of Txs causes cross coupling. Adjacent transmitting coils can be decoupled from each other by designing a suitable spacing between them [19]. Single-phase dual-receiver (Rx) coils are connected in reverse to form a three-phase DWPT system to obtain a constant voltage gain [21]. A new asymmetric coupling structure is proposed in [22], which significantly improves the stability of the output voltage in terms of horizontal, vertical, and angular displacements. A positive tetrahedral structure is proposed in [23] that can receive energy at any angle in space.

In the aforementioned planar Txs proposed for the DWPT system, cross coupling between adjacent Txs as well as mutual inductance fluctuations is unavoidable. In addition, for the existing asymmetric coupling structure is only explored in static wireless charging, however, its performance in the DWPT system is not further investigated. Therefore, based on the asymmetric coupling structure, a low-cost and low-fluctuation dual-Rx magnetic coupler is proposed in this letter. The two Rx coils consist of overlapping unipolar and solenoid coils connected in parallel to two half-bridge rectifiers, which are decoupled from each other by generating orthogonal magnetic fields. Unlike the decoupled Rx coils also used in [20], reverse windings are connected in series within the Rx coils to further smooth the variation of mutual inductance and, thus, reduce output voltage or current fluctuations. The Tx employs an I-type solenoid coil

Received 23 September 2024; revised 16 October 2024 and 19 November 2024; accepted 7 December 2024. Date of publication 11 December 2024; date of current version 28 January 2025. This work was supported in part by the National Natural Science Foundation of China under Grant 52107183 and Grant 52407197 and in part by the Natural Science Foundation of Fujian Province under Grant 2022J06011. *(Corresponding authors: Xingkui Mao; Zhongqi Li.)*

Yiming Zhang, Hangyan Zhou, Ronghuan Xie, Xingkui Mao, and Xiaoying Chen are with the Fujian Engineering Research Center of High Energy Batteries and New Energy Equipment and Systems, School of Electrical Engineering and Automation, Fuzhou University, Fuzhou 350108, China (e-mail: zym@fzu.edu.cn; 220127134@fzu.edu.cn; 230127018@fzu.edu.cn; mxk782@fzu.edu.cn; fzucxy@fzu.edu.cn).

Zhongqi Li is with the Fujian Engineering Research Center of High Energy Batteries and New Energy Equipment and Systems, School of Electrical Engineering and Automation, Fuzhou University, Fuzhou 350108, China, and also with the College of Electrical and Information Engineering, Hunan University of Technology, Zhuzhou 412008, China (e-mail: lizhongqi@hnu.edu.cn).

Color versions of one or more figures in this article are available at https://doi.org/10.1109/TPEL.2024.3516042.

Digital Object Identifier 10.1109/TPEL.2024.3516042

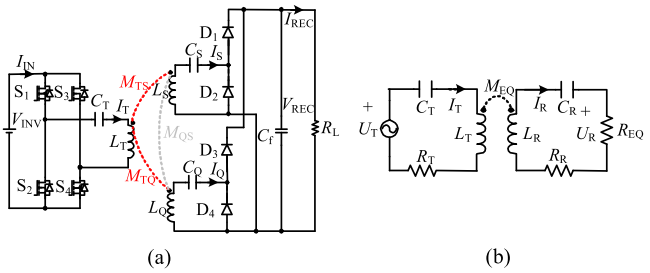

Fig. 1. Proposed DWPT system. (a) Topology. (b) Equivalent circuit.

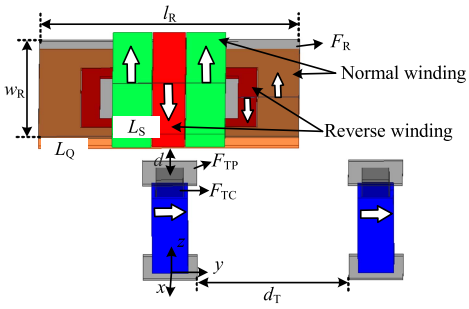

Fig. 2. 3-D view of the proposed magnetic couplers.

to enhance the magnetic field and improve the coupling, and the cross coupling between adjacent Txs is eliminated by a suitable spacing design. The optimized design of the coupler structure enables the system to achieve smooth equivalent mutual inductance fluctuations by switching the two receiving coils with each other during the dynamic charging process, which provides a stable output and improves the system's antimisalignment capability.

The rest of this letter is organized as follows. The proposed system topology is provided in Section II. The magnetic coupler structure is presented in Section III. Section IV contains the calculations and the experimental results. Finally, Section V concludes this letter.

II. Proposed System Topology

The proposed dual-Rx S-S topology is shown in Fig. 1(a). The two receiving coils L_S and L_Q are connected in parallel using series compensation and two half-bridge rectifiers. V_{INV} and I_{IN} are the input dc voltage and dc current, respectively; V_{REC} and I_{REC} are the charging voltage and the charging current, respectively; R_L is the load resistor; L_T is the Tx coil; L_S and L_Q are the Rxs; C_T, C_S, and C_Q are the series compensating capacitors for Tx and Rx. I_T, I_S, and I_Q are the currents flowing through the Tx and Rx coils; M_{TS}, M_{TQ}, and M_{QS} are the mutual inductances.

The simplified equivalent circuit of the system is shown in Fig. 1(b). Since the two receiving coils are connected in parallel, the equivalent mutual inductance M_{EQ} is the larger value of the two mutual inductances during the dynamic movement of the AGV, with the following expression:

$$M_{\mathrm{EQ}} = \max\left\{\left|M_{TS}\right|, \left|M_{TQ}\right|\right\}. \tag{1}$$

Since the two Rxs generate orthogonal magnetic fields to the Tx, the two receiving coils are decoupled, that is, $M_{SQ} = 0$. R_T and R_R are the equivalent series resistances (ESRs) of the Tx and Rx loops, respectively. U_T and U_R are the fundamental components of the inverter and rectifier ac voltages, respectively. R_{EQ} is the equivalent ac load resistance. The formulas for U_T, U_R, and R_{EQ} are

$$U_T = \frac{2\sqrt{2}}{\pi} V_{\mathrm{INV}}, \quad U_R = \frac{\sqrt{2}}{\pi} V_{\mathrm{REC}}, \quad R_{\mathrm{EQ}} = \frac{2}{\pi^2} R_L. \tag{2}$$

The WPT system operates at the resonance frequency ω_0

$$\omega_0 = \frac{1}{\sqrt{L_T C_T}} = \frac{1}{\sqrt{L_S C_S}} = \frac{1}{\sqrt{L_Q C_Q}}. \tag{3}$$

Neglecting the ESRs, the expression for the ac voltage can be obtained using Kirchhoff's voltage law as

$$I_T = \frac{R_{\mathrm{EQ}} U_T}{(\omega M_{\mathrm{EQ}})^2}, \quad I_R = \frac{U_T}{\omega M_{\mathrm{EQ}}}. \tag{4}$$

Thus, the charging voltage V_{REC}, the charging current I_{REC} at the dc side, and the output power can be expressed as

$$I_{\mathrm{REC}} = \frac{4}{\pi^2} \frac{V_{\mathrm{INV}}}{\omega_0 M_{\mathrm{EQ}}}, \quad V_{\mathrm{REC}} = \frac{4}{\pi^2} \frac{V_{\mathrm{INV}} R_L}{\omega_0 M_{\mathrm{EQ}}}. \tag{5}$$

$$P_{\mathrm{out}} = I_R^2 R_{\mathrm{EQ}} = \left[\frac{4\sqrt{2}}{\pi^2} \frac{V_{\mathrm{INV}}}{\omega M_{\mathrm{EQ}}}\right]^2 R_L. \tag{6}$$

From (6), the output power is only related to the equivalent mutual inductance when the input dc voltage and load are constant. Therefore, a smooth power output can be achieved by keeping the equivalent mutual inductance constant.

The ac–ac efficiency can be derived as

$$\eta = \frac{I_R^2 R_{\mathrm{EQ}}}{I_R^2 R_{\mathrm{EQ}} + I_T^2 R_T + I_R^2 R_R}. \tag{7}$$

III. Proposed Magnetic Coupler

The proposed magnetic coupler is shown in Fig. 2. The Tx employs an I-type solenoid coil as it has a more concentrated magnetic field and improves coupling [24]. The Rx employs a solenoid coil L_S above and a square unipolar coil L_Q stacked below, each of which has reverse windings in series to balance the variation in mutual inductance, where the arrows indicate the direction of current. When the Rx is aligned with the Tx, the transmitting coil L_T generates an upward vertical magnetic flux through the unipolar receiving coil L_Q. When the Rx coil deviates to move in the y-direction, L_T generates a horizontal magnetic flux through L_S. Since the transmitting coil L_T generates orthogonal magnetic fields through the two receiving coils, L_S and L_Q are decoupled, that is, $M_{QS} = 0$.

Define the equivalent mutual inductance volatility ΔM_{EQ} as

$$\Delta M_{\mathrm{EQ}} = \frac{M_{\mathrm{EQ\,max}} - M_{\mathrm{EQ\,min}}}{M_{\mathrm{EQ\,max}} + M_{\mathrm{EQ\,min}}}. \tag{8}$$

When the Rx is moving along the y-direction, ΔM_{EQ} is required to be as small as possible in order to have a stable output power, with a target of $\Delta M_{\mathrm{EQ}} < 5\%$ during the moving process. The size and number of turns of the magnetic coupler

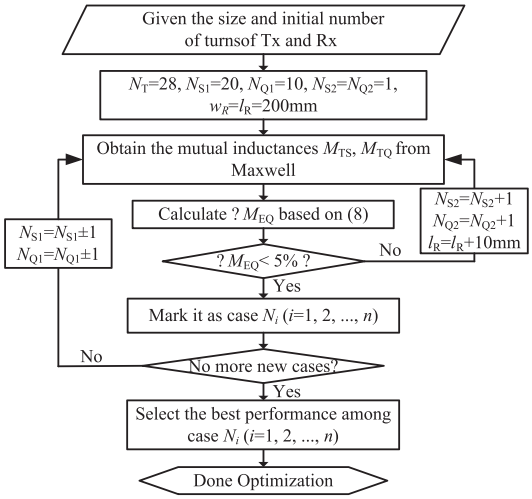

Fig. 3. Design flow of the magnetic coupling structure.

TABLE I
PARAMETERS OF THE MAGNETIC COUPLER

Description	Parameter	Value
Air gap	d (mm)	20
Length of Rx	l_R (mm)	250
Width of Rx	w_R (mm)	200
Ferrite size of Rx	F_R (mm)	250 × 200 × 2
Ferrite plate size of Tx	F_{TP} (mm)	50 × 50 × 2
Ferrite core size of Tx	F_{TC} (mm)	25 × 25 × 100
Distance between two Txs	d_T (mm)	190
Turn numbers of Tx	N_T	28
Turn number of the normal winding of L_S	N_{S1}	19
Turn number of the reverse winding of L_S	N_{S2}	7
Turn number of the normal winding of L_Q	N_{Q1}	9
Turn number of the reverse winding of L_Q	N_{Q2}	4

need to be optimized, with the optimization flowchart shown in Fig. 3. First, it is necessary to ensure that the distance between adjacent Txs is large enough to be decoupled, through simulation to obtain their optimal decoupling distance of 190 mm, with their coupling coefficients $k_{12} = 0.01$. Based on this, the initial dimensions of the Tx and the Rx and the initial number of turns of the normal winding are defined. The number of turns of the reverse winding and the length of the Rx are increased at the end of each simulation to satisfy the constraints of ΔM_{EQ}. After that the number of turns of the normal winding is added or subtracted by 1 to get a better performance combination of turns. The final parameters obtained after traversal optimization are shown in Table I.

Fig. 4 illustrates the fluctuation of each mutual inductance after optimization, where the equivalent mutual inductance M_{EQ} consists of the envelope of the absolute value of mutual inductance. The simulation results show that the fluctuation of M_{EQ} is 3.28%.

IV. EXPERIMENTAL VALIDATION

In order to verify the performance of the proposed dual-receiving coupler with smooth output, an experimental prototype is constructed, and the coils are implemented according to the

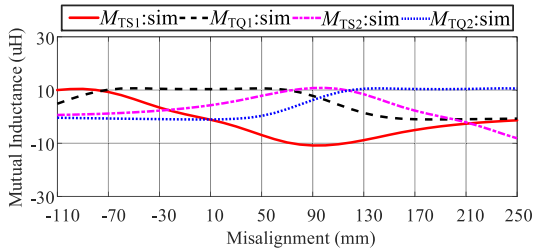

Fig. 4. Optimized mutual inductance fluctuation curves.

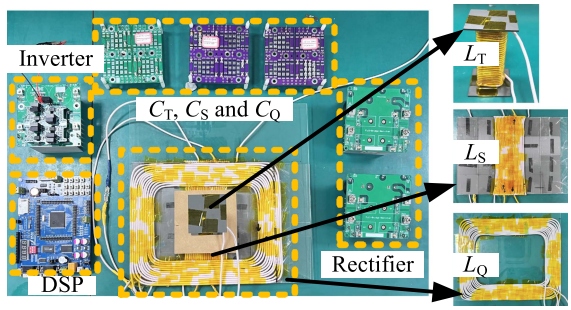

Fig. 5. Photograph of experimental prototype.

TABLE II
PARAMETERS OF THE EXPERIMENTAL PROTOTYPE

Symbol	Value	Symbol	Value	Symbol	Value
V_{INV} (V)	50 V	R_L (Ω)	20	L_Q (μH)	31.69
L_T (μH)	151.44	C_T (nF)	23.11	C_Q (nF)	110.56
L_S (μH)	52.4	C_S (nF)	66.74	–	–

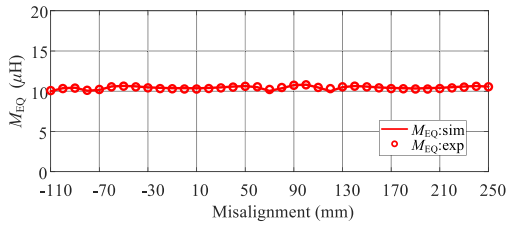

Fig. 6. Simulated and measured values of equivalent mutual inductance.

optimized parameters, as shown in Fig. 5. The parameters of the experimental prototype are shown in Table II.

The fluctuation of M_{EQ} over the moving range of two Txs is shown in Fig. 6. It can be obtained that the experimental and simulated values are highly matched, which verifies the feasibility of the optimal design of the magnetic coupler, with the maximum mutual inductance fluctuation ΔM_{EQ} of 3.6%.

Static charging was verified in 10 mm moving steps within the misalignment range. The calculated and experimental results are shown in Fig. 7. The latter Tx is the duplicate unit of the previous Tx. It can be seen that the output current and output voltage are able to remain stable with their fluctuation of 2.8%. The output power is also able to remain relatively stable within the misalignment range, with a measured fluctuation of 5.6%.

Fig. 8 shows the calculated and experimental results of load regulation, where constant current charging can be realized. The

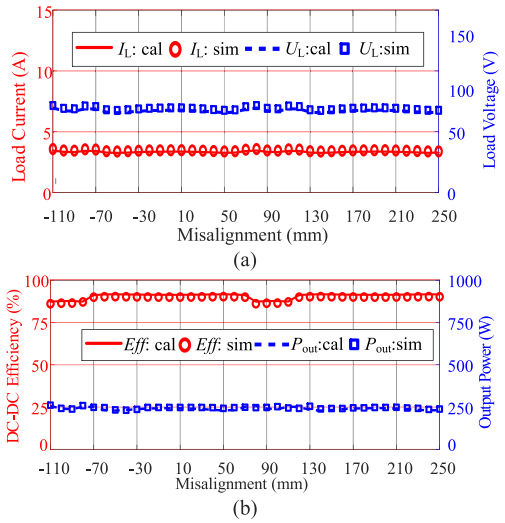

Fig. 7. Calculated and experimental results. (a) DC charging current I_{REC} and voltage V_{REC}. (b) DC–DC efficiency and output power.

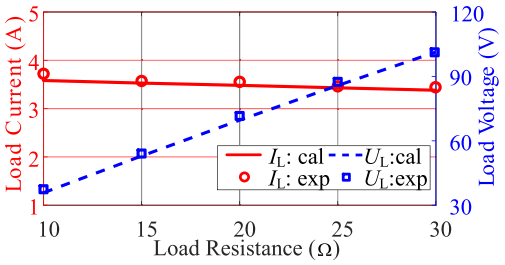

Fig. 8. Calculated and experimental results for load regulation.

TABLE III
COMPARISON WITH THE EXISTING STUDIES

Ref.	Airgap	Power capability	Efficiency	Output fluctuations
[20]	100 mm	384 W	87.6%	±2%
[21]	70 mm	500 W	92.02%	±1.17%
[22]	50 mm	200 W	91.9%	±2.83%
[24]	25 mm	1.1 kW	87.22%	±1.18%
This paper	20 mm	250 W	91.7%	±2.8%

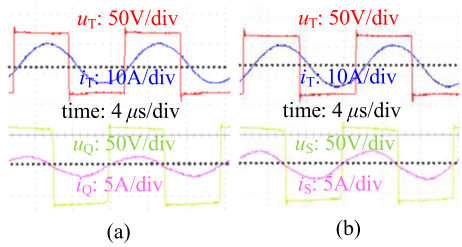

Fig. 9. Experimental waveforms. (a) When the receiving coil L_Q is operating. (b) When the receiving coil L_S is operating.

experimental waveforms are shown in Fig. 9. It can be seen that the zero-voltage switching has been achieved. Fig. 10 shows the loss distribution, with relatively high coil losses due to the use of dual-Rx coils. Experimental results show that the proposed dual-Rx magnetic coupler is capable of achieving a smooth output.

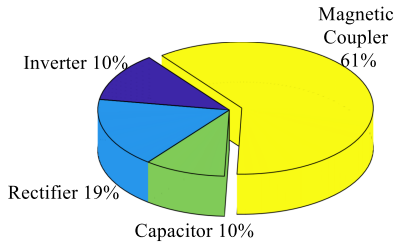

Fig. 10. Loss distribution.

The performance comparisons with previous studies are listed in Table III. It can be seen that high efficiency and smooth-output fluctuations can also be achieved using the proposed I-type solenoid Tx and dual-Rx orthogonal Rx.

V. CONCLUSION

In this article, a dual-Rx coupler applied to AGVs has been proposed to achieve a stable output during dynamic charging. The Tx utilizes an I-shaped solenoid structure that enhances the magnetic field and improves the coupling. The Rx consists of a unipolar Q-coil stacked with a solenoid coil, which is decoupled by generating an orthogonal magnetic field. The two receiving coils are connected in parallel with two half-bridge rectifiers. The optimized design of the coupler enables the system to achieve a smooth equivalent mutual inductance fluctuation by switching the two receiving coils during movement, thus reducing the output fluctuation. The experimental results validate the effectiveness of the proposed DWPT system.

REFERENCES

[1] W. Pan, R. Liu, R. Xie, Y. Zhuang, X. Mao, and Y. Zhang, "A multi-output modular wireless power transfer system with constant-current characteristic," *IEEE Trans. Power Electron.*, early access, 2024, doi: 10.1109/TPEL.2024.3512656.

[2] E. Rong, P. Sun, G. Yang, J. Xia, Z. Liu, and S. Li, "5-kW, 96.5% efficiency capacitive power transfer system with a five-plate coupler: Design and optimization," *IEEE Trans. Power Electron.*, vol. 40, no. 1, pp. 2542–2555, Jan. 2025, doi: 10.1109/TPEL.2024.3462410.

[3] Y. Zhang, H. Zhou, Z. Shen, R. Xie, Z. Zheng, and X. Chen, "A family of self-adaptive interoperable receivers based on multiple decoupled receiving poles for electric vehicle wireless charging systems," *IEEE Trans. Power Electron.*, vol. 39, no. 9, pp. 11794–11802, Sep. 2024.

[4] H. Tang et al., "A self-adaptive dual-channel LCC-S detuned topology for misalignment tolerance in AUV wireless power transfer systems," *IEEE Trans. Power Electron.*, early access, 2024, doi: 10.1109/TPEL.2024.3492194.

[5] N. U. Hassan, S.-W. Hong, and B. Lee, "A robust multioutput self-regulated rectifier for wirelessly powered biomedical applications," *IEEE Trans. Ind. Electron.*, vol. 68, no. 6, pp. 5466–5472, Jun. 2021.

[6] D. Wang, C. Fu, X. Bei, and Q. Zhao, "A reconfigurable half-bridge compensation topology-based WPT system with constant current and constant voltage outputs," *IEEE Trans. Circuits Syst. II, Exp. Briefs*, vol. 70, no. 1, pp. 256–260, Jan. 2023.

[7] C. Zhu et al., "Analysis and design of cost-effective WPT systems with dual independently regulatable outputs for automatic guided vehicles," *IEEE Trans. Power Electron.*, vol. 36, no. 6, pp. 6183–6187, Jun. 2021.

[8] R. Mai, Y. Luo, B. Yang, Y. Song, S. Liu, and Z. He, "Decoupling circuit for automated guided vehicles IPT charging systems with dual receivers," *IEEE Trans. Power Electron.*, vol. 35, no. 7, pp. 6652–6657, Jul. 2020.

[9] W. Pan, C. Liu, H. Tang, Y. Zhuang, and Y. Zhang, "An interoperable electric vehicle wireless charging system based on mutually spliced double-D coil," *IEEE Trans. Power Electron.*, vol. 39, no. 3, pp. 3864–3872, Mar. 2024.

[10] S.-J. Huang, T.-S. Lee, W.-H. Li, and R.-Y. Chen, "Modular on-road AGV wireless charging systems via interoperable power adjustment," *IEEE Trans. Ind. Electron.*, vol. 66, no. 8, pp. 5918–5928, Aug. 2019.

[11] H. Kanazawa, H. Uwai, S. Kiuchi, and H. Matsumoto, "Receiver-position-based unbalanced-current control for a three- to single-phase wireless power transfer system for AGVs," *IEEE Trans. Ind. Electron.*, vol. 70, no. 4, pp. 3245–3256, Apr. 2023.

[12] B. Yang et al., "Analysis and design of a T/S compensated ipt system for agv maintaining stable output current versus air gap and load variations," *IEEE Trans. Power Electron.*, vol. 37, no. 5, pp. 6217–6228, May 2022.

[13] C. Jiang, K. T. Chau, C. Liu, C. H. T. Lee, W. Han, and W. Liu, "Move-and-charge system for automatic guided vehicles," *IEEE Trans. Magn.*, vol. 54, no. 11, Nov. 2018, Art. no. 8600105.

[14] M. L. G. Kissin, G. A. Covic, and J. T. Boys, "Steady-state flat-pickup loading effects in polyphase inductive power transfer systems," *IEEE Trans. Ind. Electron.*, vol. 58, no. 6, pp. 2274–2282, Jun. 2011.

[15] S. Liu et al., "An output power fluctuation suppression method of DWPT systems based on dual-receiver coils and voltage doubler rectifier," *IEEE Trans. Ind. Electron.*, vol. 70, no. 10, pp. 10167–10179, Oct. 2023.

[16] S. Y. Choi, B. W. Gu, S. Y. Jeong, and C. T. Rim, "Advances in wireless power transfer systems for roadway-powered electric vehicles," *IEEE J. Emerg. Sel. Top. Power Electron.*, vol. 3, no. 1, pp. 18–36, Mar. 2015.

[17] J. Shin et al., "Design and implementation of shaped magnetic-resonance based wireless power transfer system for roadway-powered moving electric vehicles," *IEEE Trans. Ind. Electron.*, vol. 61, no. 3, pp. 1179–1192, Mar. 2014.

[18] S. Raabe and G. A. Covic, "Practical design considerations for contactless power transfer quadrature pick-ups," *IEEE Trans. Ind. Electron.*, vol. 60, no. 1, pp. 400–409, Jan. 2013.

[19] Y. Zhang, H. Zhou, Z. Shen, R. Xie, X. Chen, and X. Mao, "An interoperable dynamic wireless charging system with stable output based on a self-adaptive two-pole receiver," *IEEE Trans. Power Electron.*, vol. 39, no. 10, pp. 11943–11947, Oct. 2024.

[20] Y. Li et al., "A new coil structure and its optimization design with constant output voltage and constant output current for electric vehicle dynamic wireless charging," *IEEE Trans. Ind. Informat.*, vol. 15, no. 9, pp. 5244–5256, Sep. 2019.

[21] H. Li, Y. Liu, K. Zhou, Z. He, W. Li, and R. Mai, "Uniform power IPT system with three-phase transmitter and bipolar receiver for dynamic charging," *IEEE Trans. Power Electron.*, vol. 34, no. 3, pp. 2013–2017, Mar. 2019.

[22] Y. Yao, Y. Wang, X. Liu, Y. Pei, and D. Xu, "A novel unsymmetrical coupling structure based on concentrated magnetic flux for high misalignment IPT applications," *IEEE Trans. Power Electron.*, vol. 34, no. 4, pp. 3110–3123, Apr. 2019.

[23] X. Dai, L. Li, X. Yu, Y. Li, and Y. Sun, "A novel multi-degree freedom power pickup mechanism for inductively coupled power transfer system," *IEEE Trans. Magn.*, vol. 53, no. 5, May 2017, Art. no. 8600107.

[24] C. Zhu et al., "A magnetic field concentration enhanced I-shaped transmitter for DWPT system to achieve low power fluctuation," *IEEE Trans. Power Electron.*, vol. 39, no. 1, pp. 1690–1700, Jan. 2024.